

## Intermittency in spin-wave instabilities

J. Becker, F. Rödelsperger, Th. Weyrauch, and H. Benner\*

*Institut für Festkörperphysik, Technische Universität Darmstadt, D-64289 Darmstadt, Germany*

W. Just<sup>†</sup>

*Max-Planck-Institut für Physik komplexer Systeme, Nöthnitzer Strasse 38, D-01187 Dresden, Germany*

A. Čenys<sup>‡</sup>

*Semiconductor Physics Institute, LT-2600 Vilnius, Lithuania*

(Received 25 March 1998; revised manuscript received 14 August 1998)

The dynamics of the magnetization of yttrium iron garnet spheres was studied by ferromagnetic resonance both within the subsidiary absorption regime and the coincidence regime of the first-order Suhl instability. The absorption signal shows auto-oscillations with a rich variety of nonlinear behavior. Along with other routes to chaos we observed intermittency and identified each of the Pomeau-Manneville types I–III. Within the chaotic regime crisis-induced intermittency, on-off intermittency, and noise-induced intermittent behavior were observed. [S1063-651X(99)00602-9]

PACS number(s): 05.45.–a, 75.40.Gb, 76.50.+g

### I. INTRODUCTION

During the last two decades nonlinear dynamic phenomena have been observed experimentally in a variety of systems ranging from mechanical devices and computerlike electronic circuits to human heart and brain dynamics. Magnetic systems have extensively been investigated, e.g., by high-power ferromagnetic resonance (FMR) [1–3] for more than ten years. Most of the well-known nonlinear dynamic phenomena, as well as new ones, have been observed in these systems. Up to now, however, intermittency in FMR experiments has been reported rather scarcely in the literature [4,5]. To fill this gap we present a detailed study of various intermittent phenomena in high-power FMR experiments.

We have studied the nonlinear spin dynamics of yttrium iron garnet (YIG) spheres at the first-order Suhl instability under two physically different conditions: In the coincidence regime the parametric excitation of spin waves is affected by resonant pumping on the FMR mode, while, under subsidiary absorption conditions, the pumping frequency is well above the FMR mode, i.e., the pumping is nonresonant and requires much higher microwave power to reach the threshold for spin-wave excitation. These different types of excitation lead to physically well-distinguishable behavior above the instability threshold (Sec. II). While under subsidiary absorption the system is only weakly chaotic, with fractal dimensions in the order of 2 to 3, in the coincidence regime one often encounters chaotic behavior with attractor dimensions between 5 and 10 or even higher [6]. In the latter case, a special type of coupling between spin-wave modes leads to many internal degrees of freedom being involved in the dynamics, and the high dimensionality is manifested in typical

phenomena such as multistability and multiple time scales.

Intermittency phenomena are affected by these different excitation conditions as well. In this paper we present experimental observations and analyses on all Pomeau-Manneville intermittency types (Sec. III), crisis-induced intermittency, and on-off intermittency (Sec. IV). We present examples of how to relate the intermittency mechanisms to the underlying parametric process or directly to the specific type of nonlinear couplings between spin-wave modes (see the Appendix).

### II. HIGH-POWER FERROMAGNETIC RESONANCE AT THE FIRST-ORDER SUHL INSTABILITY

Suhl's first-order spin-wave instability [7] is based on the parametric excitation of spin waves through transverse pumping on the uniform magnetization. His theory starts from the idea of weakly coupled eigenmodes with nonlinear couplings becoming efficient only at higher amplitudes. Considering only nonlinear terms of lowest order (arising from so-called *three-magnon processes* of the corresponding Hamiltonian) a coupled set of amplitude equations for the uniform mode  $a_0$  and for the spin wave modes  $a_{\mathbf{k}}$  is obtained,

$$\begin{aligned} \dot{a}_0(t) &= -[i(\omega_0 - \omega_p) + \Gamma_0]a_0 - \sum_{\mathbf{k}\mathbf{k}'} \rho_{\mathbf{k}\mathbf{k}'}^* a_{\mathbf{k}} a_{\mathbf{k}'} - i\gamma h, \\ \dot{a}_{\mathbf{k}}(t) &= -\left[ i\left( \omega_{\mathbf{k}} - \frac{\omega_p}{2} \right) + \Gamma_{\mathbf{k}} \right] a_{\mathbf{k}} + \sum_{\mathbf{k}'} \rho_{\mathbf{k}\mathbf{k}'} a_0 a_{\mathbf{k}'}^*, \end{aligned} \quad (1)$$

where  $\omega_0$  and  $\omega_{\mathbf{k}}$  are the corresponding eigenfrequencies,  $\Gamma_0$  and  $\Gamma_{\mathbf{k}}$  are the phenomenological damping parameters,  $\omega_p$  and  $h$  are the microwave pumping frequency and amplitude,  $\gamma$  is the gyromagnetic factor, and  $\rho_{\mathbf{k}\mathbf{k}'}$ , finally, denote the nonlinear coupling coefficients, which are of dipolar origin and essentially determined by the specific type of interacting eigenmodes (see, e.g., Ref. [8]). The parametric process is characterized by the decay of the pumped uniform mode into

\*Electronic address: benner@hrzpub.tu-darmstadt.de

<sup>†</sup>Electronic address: wolfram@mpipks-dresden.mpg.de

<sup>‡</sup>Electronic address: antanas@ant.pfi.lt

two spin waves or magnetostatic modes of half the pumping frequency  $\omega_{\mathbf{k}} = \omega_p/2$  and opposite wave vectors ( $\mathbf{k}$ ,  $-\mathbf{k}$ ) according to the conservation of energy and quasimomentum. This instability can either be observed off resonance (i.e., with the pumping frequency far away from the usual ferromagnetic resonance,  $\omega_p \neq \omega_0$ ) as a *subsidiary absorption*, or directly on the FMR line ( $\omega_p = \omega_0$ ) within the *coincidence regime*. Note that in ferromagnetic spheres  $\omega_0 = \gamma H$  is proportional to the magnetic field, while  $\omega_{\mathbf{k}}$  depends in a more complicated way on  $H$  as well as on the magnetization and on the amount and orientation of wave vector  $\mathbf{k}$ .

### A. Nonresonant pumping

In view of the extremely small thresholds typical for YIG, high-power FMR experiments can, in principle, be performed with a conventional ESR spectrometer. We have studied the subsidiary absorption at about 9.3 GHz. Instead of a standard reflection-type cavity we used a bimodal transmission-type cavity of quality factor 3000, which allows a nearly complete separation of the strong microwave input power from the weak time-dependent output signal. This way the signal-to-noise ratio was improved by almost 20 dB. The squared amplitude of the driving field  $h$  at sample position is proportional to the input power  $P_{\text{in}}$ , which was supplied by a microwave generator, and the transmitted signal  $P_{\text{tr}}$  is proportional to the squared amplitude  $|a_0|^2$  of the uniform mode. By means of a digital oscilloscope and an integrating voltmeter, we recorded both the time dependence of  $P_{\text{tr}}(t)$  and its time average  $\overline{P_{\text{tr}}}$  on variation of input power  $P_{\text{in}}$  and magnetic field  $H$ . The data presented below were obtained at room temperature on a highly polished sphere of pure YIG, 0.71 mm in diameter, and the magnetic field was applied either in  $\langle 100 \rangle$  or  $\langle 111 \rangle$  orientations.

The subsidiary absorption manifests as an additional absorption structure at lower field, which is well separated from the FMR main resonance and shows a drastic broadening with increasing microwave power, accompanied by auto-oscillations and sequences of bifurcations. We have systematically analyzed [6] the dynamic behavior of the subsidiary absorption signal at fixed pumping frequency, as presented in Fig. 1. The lower line shows the dependence of the Suhl threshold on  $H$  (the so-called *butterfly curve*). (Here and in the corresponding figures below,  $P_{\text{in}}$  was normalized to the minimum threshold.) The broad bumps at 1.6 and 1.9 kOe have been explained by the interaction with elastic or magnetostatic modes [9]. The next line indicates a Hopf bifurcation, and corresponds to the onset of auto-oscillations. Further bifurcation lines above separate regimes of different time behavior, e.g., period doublings, quasiperiodicity, intermittency, or chaos. The steep increase of the threshold at 2.2 kOe indicates that the bottom of the spin-wave band becomes larger than  $\omega_p/2$ , and the parametric excitation of spin waves is no longer efficient.

### B. Resonant pumping

Resonant pumping of both the uniform FMR mode and a spin-wave pair ( $\omega_p = \omega_0 = 2\omega_{\mathbf{k}}$ ) is restricted to a limited frequency range. In the case of YIG spheres, this coincidence regime ranges from 1.8 to 3.4 GHz (680–1280 Oe for  $H \parallel \langle 100 \rangle$ ). For lower field the FMR vanishes due to the oc-

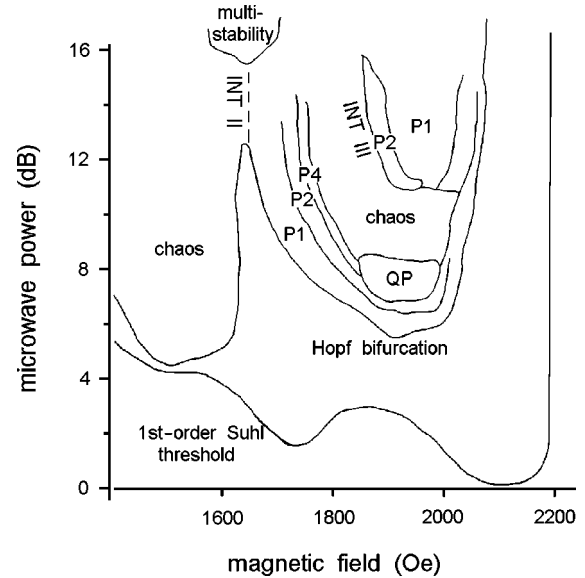


FIG. 1. Dynamics in the subsidiary absorption regime ( $\nu = 9.26$  GHz) with respect to magnetic field  $H$  and input microwave power  $P_{\text{in}}$ . The lowest line indicates the Suhl threshold, and the lines above separate regimes of different time behaviors, e.g., period doublings (P2,P4), quasiperiodicity (QP), or chaos. Intermittency is observed in several parameter regimes, e.g., type II at 1650 Oe and 12–15 dB, type III at 1900 Oe and 11–15 dB, and crisis-induced intermittency at 1900 Oe and 16 dB.

currence of magnetic domains. For higher field  $\omega_0$  falls below the spin-wave band and, keeping the resonance condition  $\omega_p = \omega_0$ , a changeover to the second-order instability takes place.

Owing to the resonant pumping condition, the fixed pumping frequency of a microwave cavity would also fix the magnetic field, i.e., would restrict the role of  $H$  as an independent control parameter. However, profiting by the resonance amplification of the FMR mode, experiments in the coincidence regime require much less microwave power to reach the instability threshold (typically some 10  $\mu\text{W}$  for high-quality YIG samples). So, for our experiments in the coincidence regime we preferred a broadband (1–4 GHz) transmission-type setup described elsewhere [2], which allows a variation of  $\omega_p$  simultaneously with  $H$ . Instead of a microwave cavity, we used two microcoils with perpendicular orientation in order to minimize mutual disturbances by crosstalk. The signal transmitted to the pickup coil was amplified, detected by a diode, and recorded in a similar way as described above.

For resonant pumping within the coincidence regime the first-order Suhl threshold shows up as a sharp and asymmetric break at the top of the FMR. With increasing input power the break becomes broader and may be followed by further breaks, resulting in a complex multistability (see Fig. 2). This multistability is connected with a variety of auto-oscillations. Details have been presented in the literature and have been explained in terms of a multimode model including the specific properties of discrete magnetostatic modes in the parametric process [8,10,11]. According to this model the sudden jumps from one level to another are induced by the nonlinear coupling or decoupling of certain spin-wave modes.

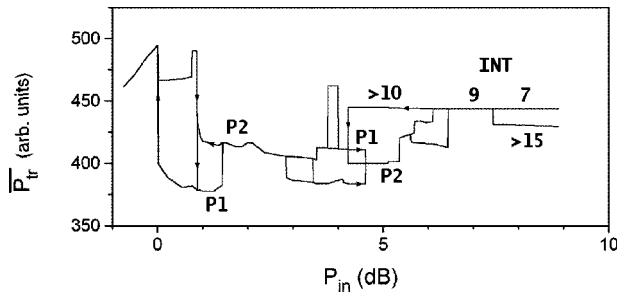


FIG. 2. Multistability in the coincidence regime ( $\nu = 2.37$  GHz,  $H = 840$  Oe). The averaged transmitted power  $\overline{P}_{tr}$  is plotted vs the input power  $P_{in}$  (normalized to the Suhl threshold). Different dc levels correspond to different types of dynamics. Periodic behavior is indicated by its periodicity (P1,P2), and chaotic behavior by the attractor dimension (accuracy  $\pm 1$ ). Chaos-chaos intermittency is observed at the upper chaotic level (INT).

### C. Observed routes to chaos

As a general result, we found that a global correspondence to one of the well-known scenarios of Feigenbaum, Ruelle, Takens, and Newhouse, or Pomeau and Manneville [12] does not occur, but a variety of parts from all of them. This obviously corresponds to the fact that the nonlinearities of a real system are more complicated and based on a larger number of internal degrees of freedom than those of the simple models from which these standard routes have been derived. The physical meaning of the degrees of freedom is probably that of specific eigenmodes or a collective motion of several of them.

Quasiperiodicity with up to three fundamental frequencies was observed both in subsidiary absorption (cf. Fig. 1) and in the coincidence regime. In the latter case, for instance, closely above the threshold the FMR signal starts to auto-oscillate with typical frequencies ranging from 100 to 400 kHz. A few dB above, a second fundamental frequency occurs—corresponding to a second Hopf bifurcation—together with several mixing frequencies and harmonics, which indicate that the attractor is a 2 torus. Very seldom, we also found a third fundamental frequency occurring within an extended parameter range. More often, instead of a third Hopf bifurcation and a collapse of the resulting 3 torus to chaos [13] we observed the spin system switch over to a coexisting stable attractor.

The changeover to chaos was generally accompanied by a jump of  $\overline{P}_{tr}$ , but did not arise from a 2 or 3 torus. Hence it could not be related to a Ruelle-Takens-Newhouse scenario. Instead we suppose that the chaotic behavior results from a sudden increase of the number of coupled modes, which is related to some global symmetry-breaking bifurcation [6] and does not follow one of the standard routes.

Period-doubling routes, as reported previously from both transverse and parallel pumping experiments [14,15], were observed up to period 8, but occurred rather seldom. Very scarcely we even observed a sequence of *period triplings* (not to be confused with a period-3 window) up to period 9. More often, however, only a single period doubling was found, which remained stable for a rather extended parameter range and then changed directly over to chaos. Though the Feigenbaum route is known to be very sensitive to noise which might have suppressed further period doublings, we

rather interpret the observed behavior to represent an independent route.

Intermittency was observed in several parts of parameter space, in subsidiary absorption as well as in the coincidence regime. A detailed study of the intermittent routes to chaos, and various types of the intermittent behavior inside the chaotic regime are the subjects of the following sections.

## III. POMEAU-MANNEVILLE INTERMITTENCY

Pomeau-Manneville intermittency occurs in conjunction with a bifurcation where a formerly stable periodic motion (i.e., a limit cycle) becomes unstable [16]. In a suitable Poincaré section this is equivalent to a stable fixed point becoming unstable via a codimension-1 bifurcation. The fixed point of a one-dimensional map can become unstable via a local bifurcation in three basically different ways: the eigenvalue crossing the unit circle at  $+1$ , two complex conjugate eigenvalues crossing the unit circle simultaneously, and the eigenvalue crossing the unit circle at  $-1$ . The three types of Pomeau-Manneville intermittency correspond to these three different bifurcations.

All these types of “classical” intermittency have been observed in a large variety of experimental situations. As far as we know, however, high-power FMR in YIG spheres represents the only physical system where all three types of intermittency can be observed with a single experimental setup. While the phenomenological analysis of our data yields convincing evidence for each intermittency type, the physical understanding of their mechanisms in terms of spin-wave dynamics is less obvious [17] and highly nontrivial. In order to obtain an idea of the physical background, we tried to relate these specific bifurcations to the underlying parametric spin-wave excitation described by Eq. (1). As an example, in the Appendix we present the physical conditions for the occurrence of a subcritical Hopf bifurcation, which is characteristic of the second one of these types.

### A. Intermittency of type I

Type-I intermittency is related to a tangent bifurcation where stable and unstable fixed points merge. Slightly above the bifurcation the Poincaré map contains a narrow channel near the merging point. Then the system evolves through this channel, and the dynamics is almost periodic with amplitudes showing a monotonous s-shaped increase with minimal slope at the center of the channel. Figure 3 shows two experimental time series representing different manifestations of this type of behavior.

The simplest map exhibiting type-I intermittency is given by

$$x_{n+1} = \epsilon + x_n + x_n^2, \quad (2)$$

where  $\epsilon > 0$  is the distance in parameter space from the bifurcation point. In order to reconstruct a corresponding map from a time-continuous system, which is in general much more complex, one has to find or construct an appropriate system variable which allows the reduction to a map. We have reconstructed such a map from both experimental time series of Fig. 3 in a different way. The upper series represents a manifestation of type I which is observed more fre-

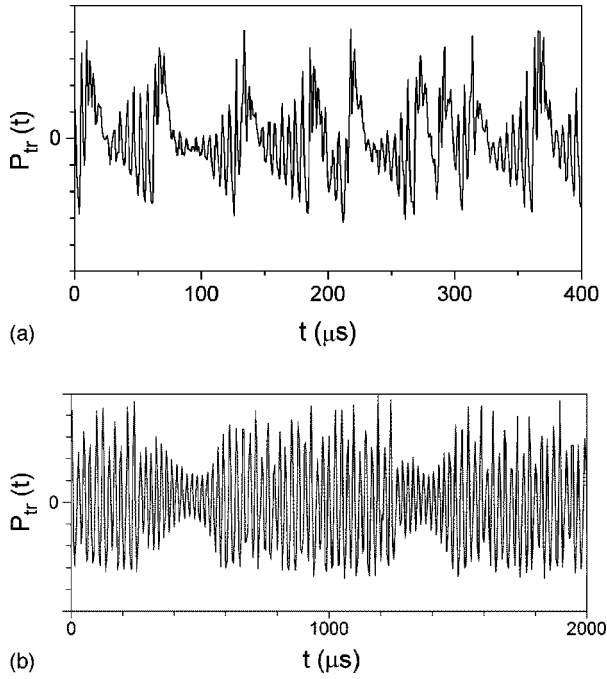


FIG. 3. Examples of time series showing type-I intermittency. Top:  $\nu=2.414$  GHz,  $H=840$  Oe, and  $P_{in}=0.66$  dBm. Laminar intervals are characterized by increasing oscillation amplitudes and interrupted by short chaotic bursts. Bottom:  $\nu=2.496$  GHz,  $H=840$  Oe, and  $P_{in}=7.04$  dBm. The laminar intervals correspond to ‘channels’ of small-amplitude oscillations separated by large-amplitude chaotic intervals of long duration.

quently in experimental systems. An appropriate return map is constructed by simply taking the local maxima as  $x_n$ . The lower time series exhibiting decreasing and reincreasing amplitudes reflects the periodic channels in a more involved way. Here we took the increment of the oscillation amplitudes rather than directly the maxima. Figure 4 shows the return map reconstructed from the lower data set of Fig. 3 together with the corresponding parabola which was obtained from a least square fit.

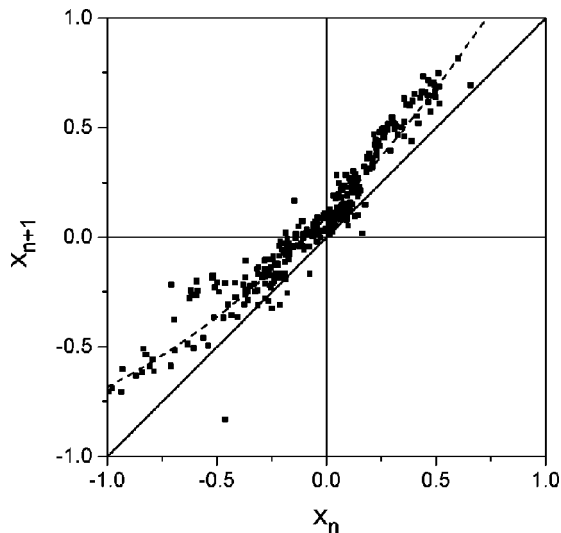


FIG. 4. First-return map extracted from the time series of Fig. 3 (bottom). The dashed line is a fit to the quadratic map [Eq. (2)], generic for type-I intermittency:  $x_{n+1}=0.092+1.045x_n+0.273x_n^2$ .

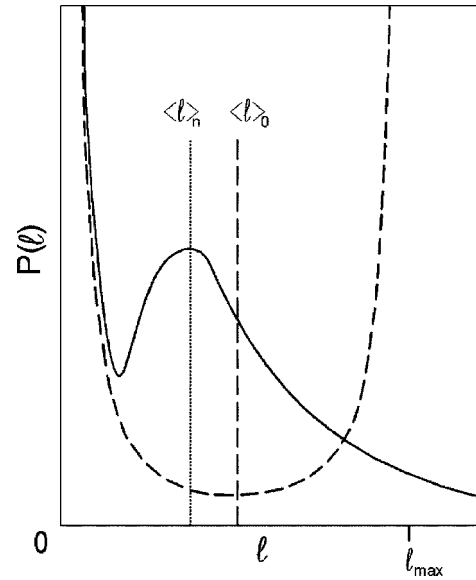


FIG. 5. Influence of noise on the distribution of laminar lengths for type-I intermittency after Ref. [18]. The dashed line gives the theoretical result in absence of noise, and the solid line results from a simulation with additional noise. The latter distribution is exponential for large  $l$ , and the mean length  $\langle l \rangle$  is shifted to a smaller value.

Assuming the reinjection to the channel region to be homogeneous and uncorrelated, it is possible to calculate the statistical distribution of the laminar lengths, i.e., the lengths of the time intervals during which the system behaves in a periodic manner. The theoretical distribution exhibiting square-root singularities at zero and at a maximum length  $l_{max}$  is given by the dashed curve in Fig. 5. Moreover, the mean value of the laminar lengths  $\langle l \rangle$  is expected to scale with the deviation from the critical point  $\epsilon$  like  $\langle l \rangle \sim \epsilon^{-1/2}$ .

The most characteristic feature of this distribution is the strict cutoff at  $l_{max}$ . To compare this result with experimental data, however, one has to take into account that the dynamics of real systems is always affected by noise. Type-I intermittency has turned out to be very sensitive to the presence of noise, which becomes most evident when looking at the distribution of laminar lengths. The full curve in Fig. 5 demonstrates how this distribution is affected by noise. The strict cutoff at  $l_{max}$  is smeared out, and a long exponential tail evolves reflecting the fact that now arbitrarily long residence times become possible.

We have developed a computer program which allows one to separate laminar and chaotic intervals of the time series in an intelligent way. The program includes the application of several operations on the whole data set, e.g., different types of local averaging, numerical differentiation, subtraction of subsequent extrema, etc., which allow one to transform the data set in a way that the two different states (here laminar and chaotic) can be separated by fixing some boundary line. By determining the lengths of the time intervals between two subsequent crossings of this line, one obtains statistics for the laminar state and for the chaotic state, respectively. The distribution of the laminar lengths obtained from experimental data sets like that of Fig. 3 is shown in Fig. 6. The similarity with the simulated noisy distribution of Fig. 5 is obvious.

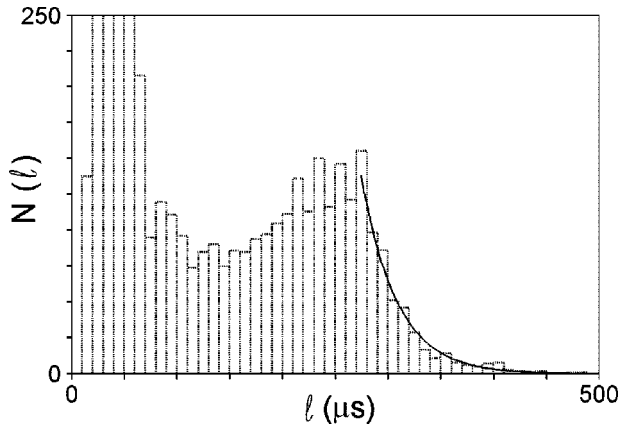


FIG. 6. Experimental distribution of laminar lengths of the time series shown in Fig. 3. The data set consisted of  $7.5 \times 10^5$  data points. The solid line is a fit to the exponential tail of the distribution.

### B. Intermittency of type II

Type II is related to a subcritical Hopf bifurcation, i.e., when the formerly stable fixed point in the Poincaré section becomes unstable via collision with an unstable limit cycle. As a result, the system spirals out of the vicinity of the fixed point. To describe this type of dynamics at least a two-dimensional map is needed, and a first-return map of a single coordinate does not give reliable information, in contrast to the previous case. Close to the bifurcation point two different periodicities appear in the system dynamics: one representing the period of the system piercing the Poincaré plane, and the other reflecting the spiral motion, which can in first approximation be considered as the period of the former unstable limit cycle.

In the experimental time series (Fig. 7), the first one corresponds to the carrier frequency and the second one shows up indirectly via the slow beat which appears most pronounced in the long periodic phases. These two frequencies, together with a variety of harmonics and mixing frequencies, are clearly manifested in the spectrum presented in Fig. 8.

The experimental distribution of the laminar lengths together with the best fit to the theoretical distribution function [12],

$$N(l) \sim \frac{\epsilon^2 e^{4\epsilon l}}{(e^{4\epsilon l} - 1)^2}, \quad (3)$$

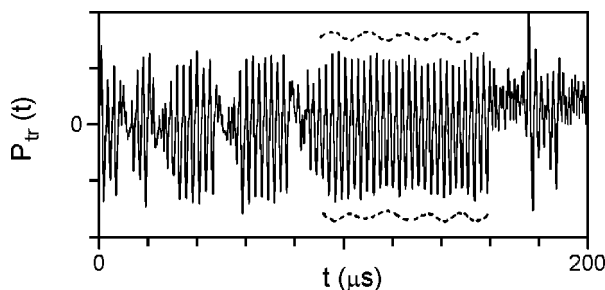


FIG. 7. Example of a time series showing type-II intermittency.  $\nu = 9.257$  GHz,  $H = 1590$  Oe, and  $P_{in} = 15$  dB. The laminar intervals are quasiperiodic, the low-frequency amplitude modulation has been stressed by the dashed envelopes.

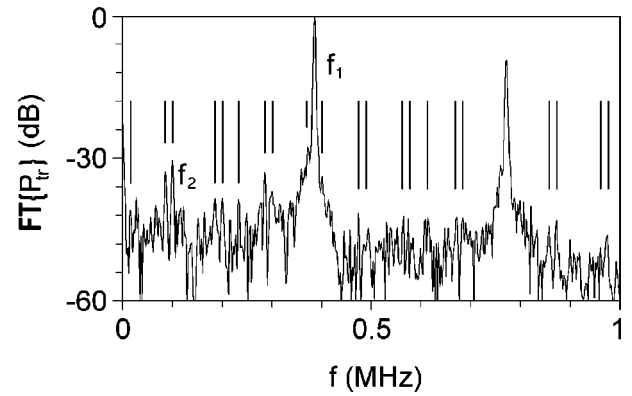


FIG. 8. Fourier spectrum of the time series shown in Fig. 7. Two fundamental frequencies occur at  $f_1 = 385$  kHz and  $f_2 = 100$  kHz. All strongest spectral components, indicated by vertical bars, were identified to present mixing frequencies  $mf_1 + nf_2$ ,  $m, n$  integer,  $|m| \leq 3$  and  $|n| \leq 10$ . The frequency splitting  $\Delta = 4f_2 - f_1 = 15$  kHz occurring everywhere in the spectrum reflects the amplitude modulation of the time series.

is shown in Fig. 9.

In this case the influence of noise seems to be much less important than for type I. The magnetic-field dependence of the mean laminar length in Fig. 10 is in very good agreement with the theoretical power law  $\langle l \rangle \sim \epsilon^{-1}$  with  $\epsilon = |H - H_c|$ .

### C. Intermittency of type III

Type-III intermittency occurs in conjunction with an inverse period-doubling bifurcation, i.e., when the stable fixed point becomes unstable via the collision with an unstable period-2 orbit. If the fixed point occurs at zero, the system will evolve out of the region around it by alternating between positive and negative values with growing amplitude. The first-return map close to the fixed point is given by

$$x_{n+1} = -(1 + \epsilon)x_n - ux_n^3. \quad (4)$$

In the continuous time domain one observes the strictly periodic motion becoming unstable toward oscillation with alternating sign and growing amplitude. An example of an experimental time series and the reconstructed return map are shown in Figs. 11 and 12, respectively.

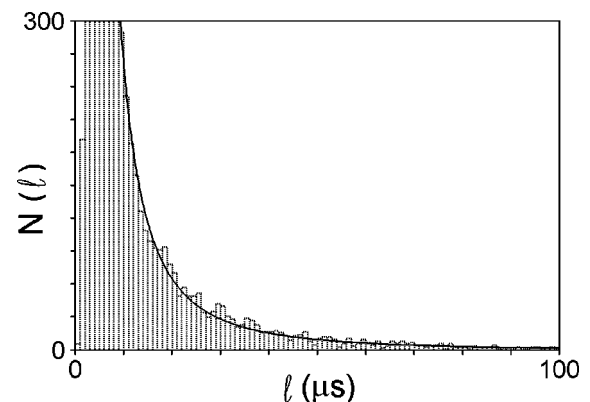


FIG. 9. Experimental distribution of the laminar lengths.  $\nu = 9.255$  GHz,  $H = 1592$  Oe, and  $P_{in} = 15.5$  dB. The solid line is a fit to the theoretical distribution for type-II intermittency, Eq. (3).

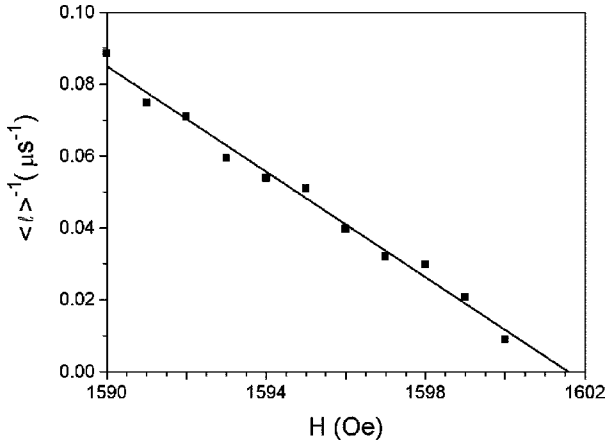


FIG. 10. Inverse mean laminar length  $\langle l \rangle^{-1}$  vs magnetic field  $H$ . The solid line represents a least square fit to a linear dependence and yields  $H_c = 1601.5$  Oe.

The laminar intervals of the original signal show the typical spreading up of successive maxima. In order to extract this part of the signal, we have recorded the sliding average over exactly one period (Fig. 11, bottom). Thus the dominating period-1 component is suppressed, while the period-2 component is retained and can be further analyzed by proper algorithms. Note that successive maxima  $\hat{x}_n$  of the averaged signal occur at double period. Using these maxima for constructing a first-return map, as done in Fig. 12, is, in fact, equivalent to a second-return map of the original time signal. This means, e.g., that an alternating sign characteristic of the negative eigenvalue of the respective bifurcation is absent from this map. The map shows the expected nonlinear increase, fitted by a cubic parabola, together with a horseshoe-shaped chaotic repeller responsible for reinjection. The experimental distribution of the laminar lengths fits well the theoretical result [12]:

$$N(l) \sim \frac{\epsilon^{3/2} e^{2\epsilon l}}{(e^{2\epsilon l} - 1)^{3/2}}. \quad (5)$$

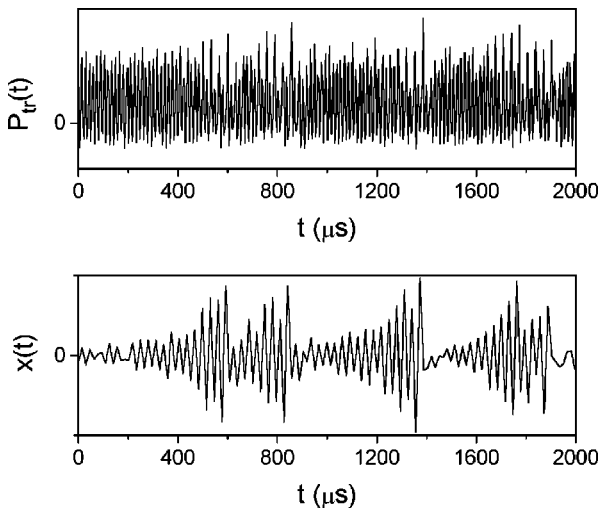


FIG. 11. Example of a time series showing type-III intermittency.  $\nu = 2.385$  GHz,  $H = 800$  Oe, and  $P_{\text{in}} = 8.49$  dBm. Top: original signal; the laminar intervals exhibit the typical spreading up of successive maxima. Bottom: same signal averaged over one period.

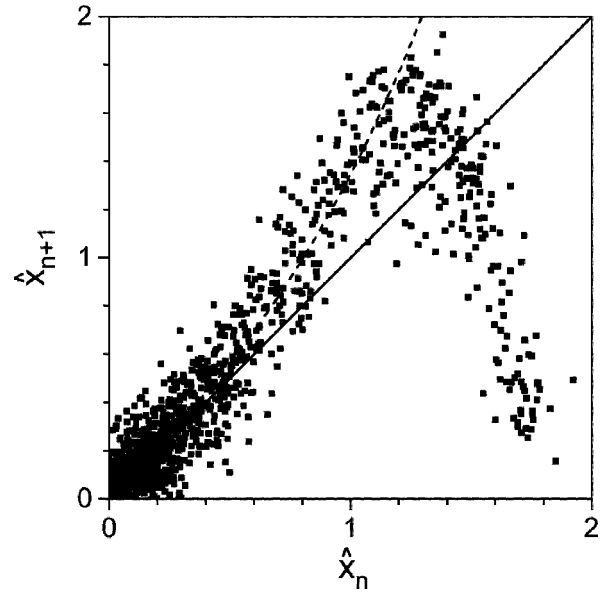


FIG. 12. First-return map extracted from the time series of Fig. 11 (bottom). The dashed line is a fit to the second iterate of Eq. (4) generic for type-III intermittency:  $x_{n+2} = 1.056x_n + 0.291x_n^3$ . In order to exclude the reinjecting part of the map, our fit was restricted to  $x_n \leq 1.2$ .

In Fig. 13, instead of  $N$ , we have compared the integrated distribution which is less sensitive to noise, but more sensitive to systematic deviations.

#### IV. CHAOS-CHAOS INTERMITTENCY

In our experiment, the majority of intermittency phenomena is not of Pomeau-Manneville type. More often, one encounters intermittent transitions between different types of chaotic behavior within the chaotic regime. We have identified different types of this behavior.

##### A. Crisis-induced intermittency

This type of chaos-chaos intermittency was described by Grebogi, Ott, and Yorke [19,20] and related to the occurrence of a crisis, which means the local collision of one or two chaotic attractors with an unstable periodic orbit. Either

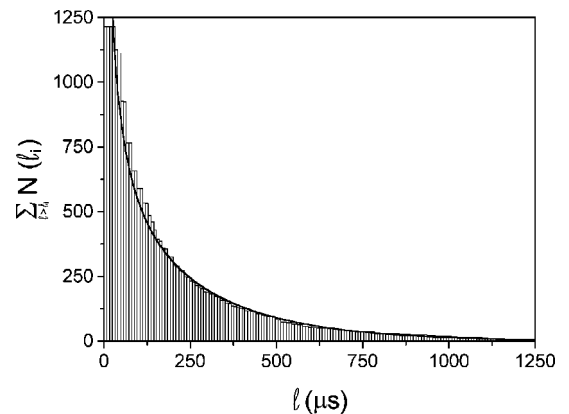


FIG. 13. Integrated experimental distribution of the laminar lengths. The solid line is a fit to the theoretical distribution for type-III intermittency.

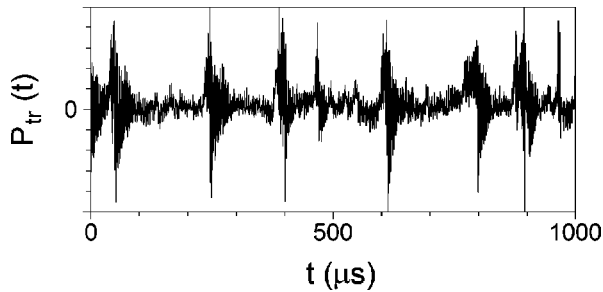


FIG. 14. Time series representing a homoclinic crisis at  $\nu = 9.258$  GHz,  $H = 1877$  Oe, and  $P_{in} = 16.5$  dB (cf. Fig. 1).

the merging of two formerly separate stable chaotic attractors or the abrupt widening of an attractor leads to intermittent jumps between the two attractor regions. Typical experimental time series are shown in Figs. 14 and 15.

The three extended plots of chaotic bursts show strong similarities in their initial phase, which directly reflects the local character of the underlying bifurcation: the trajectory always escapes from the former chaotic attractor at the same phase space area where the collision with the unstable periodic orbit takes place. The unstable periodic orbit generally represents a large amplitude oscillation. Here the first few increasing oscillations of the bursts characterize the contracting phase where the trajectory approaches the orbit along the stable manifold. The following decreasing oscillations correspond to the expanding phase where the trajectory is repelled along the unstable manifold, ending up again at the former chaotic attractor. This indicates that we are dealing with a homoclinic crisis. The duration of the expanding phase of the orbit was found to be definitely longer than the contracting phase, which is consistent with the fact that in dissipative

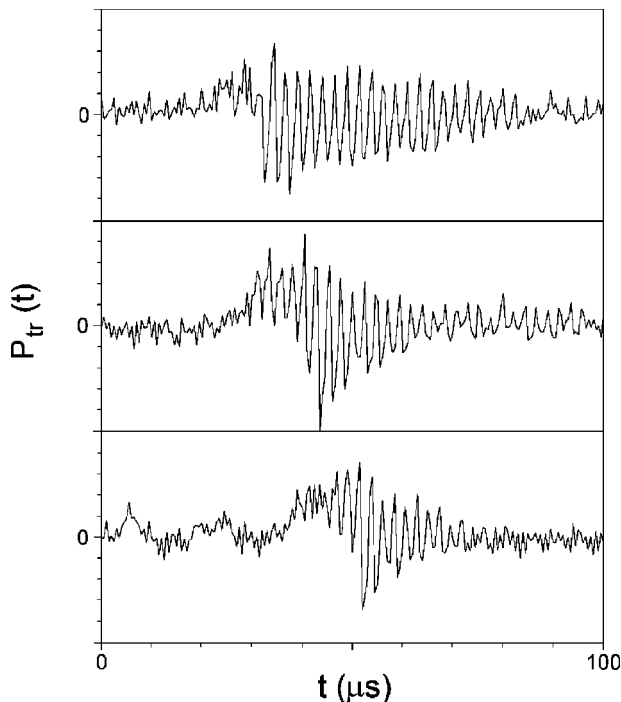


FIG. 15. Extended plot of the chaotic bursts. The input microwave power  $P_{in}$  amounts to (from top to bottom) 15.5, 16.5, and 17.0 dB.

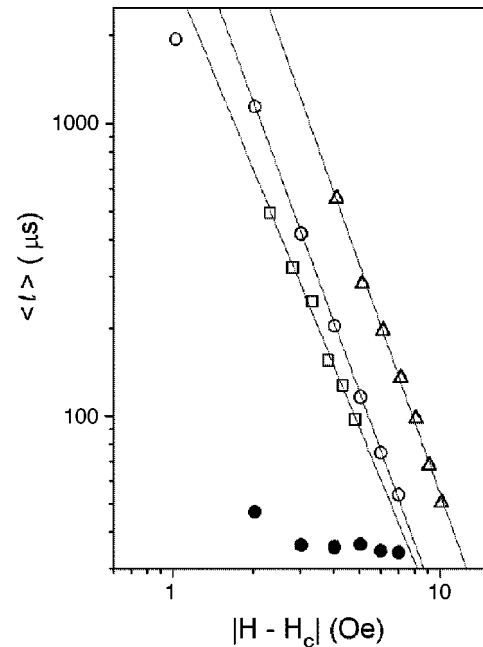


FIG. 16. Scaling behavior of the mean “laminar” length with respect to the magnetic field. Data were taken at three different microwave powers: 15.5 dB ( $\square$ ), 16.5 dB ( $\circ$ ), and 17.0 dB ( $\triangle$ ). The double-logarithmic plot yields scaling exponents  $\gamma = 2.2, 2.5$ , and 2.6, respectively. Bullets denote the mean length of the bursts for  $P_{in} = 16.5$  dB, which is nearly field independent.

systems the amount of the unstable exponents has to be smaller than the amount of the stable exponents. The variation of input power leaves the initial part of the bursts unchanged and only affects the duration of the bursts.

If the chaotic mixing within the attractor is sufficiently fast, i.e., the system “forgets” initial conditions faster than the average residence time, the distribution of the lengths is expected to be exponential. Specific properties of the dynamic system show up in the dependence of the mean laminar length on the deviation from the critical point  $\epsilon$ . Here one finds the power law  $\langle l \rangle \sim \epsilon^{-\gamma}$ , with the exponent  $\gamma$  being system dependent [21]. The value of  $\gamma$  depends on the Lyapunov exponents of the system, eigenvalues of the unstable periodic orbit participating in the crisis, and on the type of the crisis. For both homoclinic and heteroclinic crises analytical expressions for the exponent  $\gamma$  are given in Refs. [6,21]. Note that the value of  $\gamma$  is generally noninteger. Experimentally obtained power laws are shown in Fig. 16.

We tried to check the consistency of the obtained scaling exponents with theoretical predictions by estimating the contracting and expanding eigenvalues  $\beta_s$  and  $\beta_u$  for the unstable periodic orbit. In view of the low dimensionality of chaos in subsidiary absorption, a two-dimensional Poincaré section seems adequate to characterize the stability of this orbit. For the present case of a homoclinic crisis we have [6]

$$\gamma \approx \frac{1/2}{1 - \tau_s/\tau_u}, \quad (6)$$

where  $\tau_i^{-1} \equiv |\ln|\beta_i||$ ,  $i = s, u$ , denote the characteristic contraction and expansion rates, respectively. It is tempting to correlate these rates with the duration of increasing and de-

creasing amplitudes of the bursts in Fig. 15. Unfortunately, the few noisy contracting cycles do not allow a reasonable estimation of  $\tau_s$ . Looking for an independent estimate of  $\tau_s$ , we made the additional and very restrictive assumption that the total dissipation is not heavily affected by small changes of  $P_{in}$ . Then the sum of both rates can be considered as a constant,  $\tau_s^{-1} + \tau_u^{-1} = \text{const}$ , which may be obtained by fitting Eq. (6) to one of the values of  $\gamma$ . Then the other scaling exponents can be checked independently from this constant and from the respective experimental values of  $\tau_u$  only. It is clear that we cannot expect quantitative agreement from such a rough estimation, but the tendency of variation [ $\gamma = 1.4$ , 2.5 (fitted), and 2.7] is in accordance with the experimental values of Fig. 16. A more reliable comparison has to be based on the complete phase space reconstruction of the trajectory in the vicinity of the orbit, but this would be beyond the scope of our paper.

### B. On-off intermittency

On-off intermittency [22–24] occurs at a global symmetry-breaking bifurcation called *blowout bifurcation* by Ott and Sommerer [25]. At this bifurcation the formerly stable invariant manifold loses its stability, and the system dynamics extends to additional dimensions of the phase space. If the dynamics on the manifold is irregular due to a chaotic attractor or noise, and if there are no other attractors outside the manifold, on-off intermittency occurs above the blowout bifurcation point. Statistical properties of the on-off intermittency can be obtained from the simple map

$$x_{n+1} = ay_n x_n, \quad (7)$$

where  $x_n$  defines the distance from the invariant manifold,  $y_n$  describes the dynamics on the manifold, and  $a$  is a control parameter. For real systems, nonlinear terms and additive noise have to be included, but the particular properties of both of them are not important (see, e.g., Ref. [26,27]). The theoretical analysis predicts for the distribution of the ‘‘laminar’’ lengths as well as for the dependence of the mean laminar length on the deviation of  $a$  from the critical point power-law scalings with the exponents  $-\frac{3}{2}$  and  $-1$ , respectively [28]. These exponents coincide with the scaling exponents for type-III intermittency, demonstrating some similarity between these two cases, while the physical background is essentially different. The difference can also clearly be seen from experimental time series exhibiting irregular behavior in both laminar and burst phases.

We reported on-off intermittency in spin-wave instabilities in Ref. [29]. A significant criterion was to look for chaos-chaos intermittency with proper scaling exponents. A typical time series is presented in Fig. 17, and experimental power-law scalings are shown in Figs. 18 and 19. The recently predicted symmetry between laminar and burst phases [30,31] has not yet been observed in our experiment, probably due to problems with the distinction of long burst phases from noisy experimental data.

An essential feature of on-off intermittency is the additional degree of freedom which becomes unstable via a global symmetry-breaking bifurcation. The underlying physical mechanism is probably that of the transitory excitation of an additional spin-wave mode through a three-magnon process

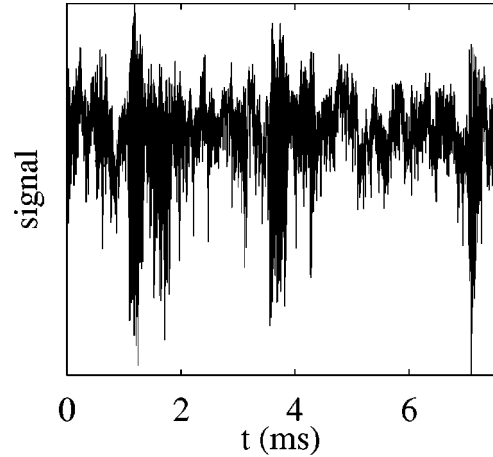


FIG. 17. Time series showing on-off intermittency in the coincidence regime ( $\nu = 2.388$  GHz,  $H = 802.5$  Oe, and  $P_{in} = 14.5$  dBm).

[6,32]. In our experimental system this additional degree of freedom could be a pair of spin waves at half the pumping frequency. The excitation of such a pair, which is of zero amplitude below the bifurcation point, is in complete analogy with the excitation of the first, critical spin-wave pair at the Suhl threshold. Thus we assume that at low microwave power, as well as within the highly chaotic regime, symmetry-breaking bifurcations dominate the system dynamics. This presumption is confirmed by the fact that the type of nonlinear coupling is the same for the spin-wave system [29,32] and for the model systems exhibiting on-off intermittency [Eq. (7)]. This coupling is bilinear in the amplitude of the additional mode and in the (nonzero) chaotic mode which is already excited. (For a more detailed discussion see the Appendix.)

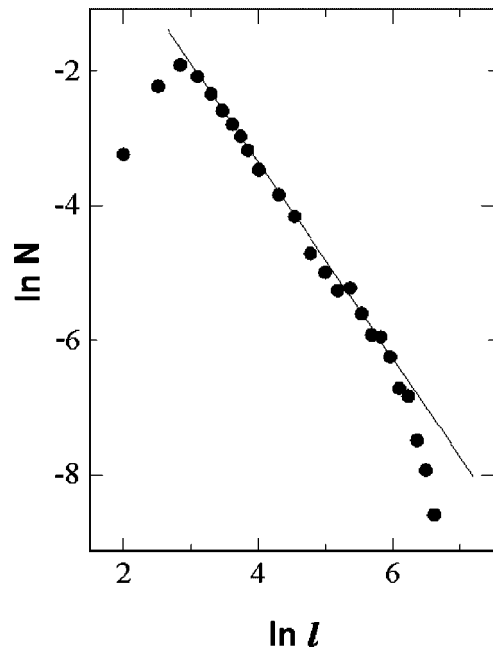


FIG. 18. Distribution of the laminar lengths, i.e., the time intervals between two bursts, from the time series shown in Fig. 17.  $l$  is measured in  $\mu\text{s}$ . The solid line corresponds to a power-law scaling of  $-\frac{3}{2}$ .

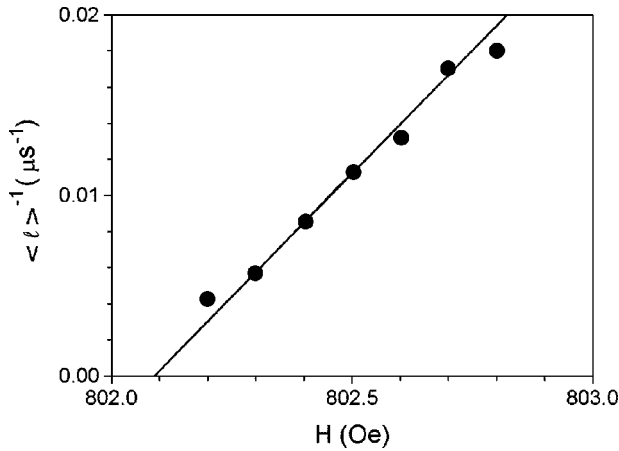


FIG. 19. Dependence of the inverse mean laminar length on magnetic field. The straight line fitted to the data corresponds to the scaling exponent  $-1$ , and yields the bifurcation point  $H_c = 802.09$  Oe.

### C. Noise-induced phenomena

In the chaotic regime of our experiment we have observed not only crisis-induced and on-off intermittency. In some cases we were unable to identify the bifurcation responsible for the occurrence of intermittency. An example of such a time series is shown in Fig. 20.

We suppose that this behavior can be related to the noise-induced hopping between several attractors in systems exhibiting multistability [33]. In that situation, the system has two or more stable states for the same set of external parameters (see Fig. 2). By additional noise, the system leaves from time to time the basin of attraction of the original state and enters that of another attractor. This happens more easily in a situation when the boundaries of the basin are fractal and riddled, i.e., closely interwoven. Then, under the influence of noise, the system wanders irregularly between several attractors. Since in the time domain this behavior shows a strong similarity to the other types of intermittency, this phenomenon is called *noise-induced intermittency*. Assuming that the probability to leave the attractor per time unit is constant, the lengths of the time intervals the system spends on one attractor obey an exponential distribution. This result is in accordance with our experimental findings (Fig. 21).

Noise-induced intermittency may be used to obtain more information on the system dynamics. By adding noise to a multistable system the intermittent jumping between coexist-

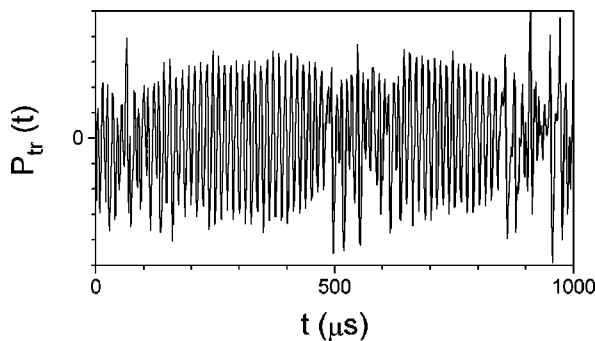


FIG. 20. Intermittent time series measured in the coincidence regime ( $\nu = 2.389$  GHz,  $H = 840$  Oe, and  $P_{in} = 7$  dBm).

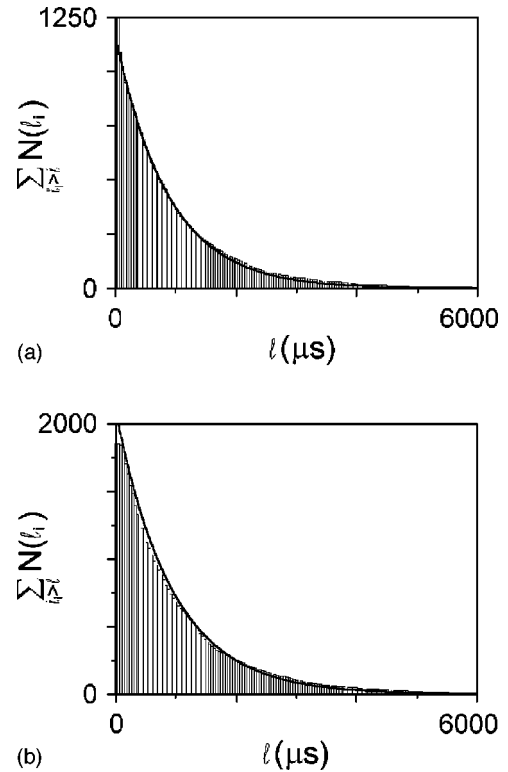


FIG. 21. Integrated distribution of the laminar (top) and chaotic (bottom) lengths for the time series shown in Fig. 20. The solid lines are fits to an exponential distribution expected for noise-induced intermittency.

ing attractors can externally be induced. The analysis of the mutual transition rates could give further insight into the topology of the system. Current work on this topic is in progress [34].

### V. CONCLUSION

We have presented the observation and detailed analysis of intermittency in high-power FMR experiments on yttrium iron garnet spheres. A large variety of intermittent behaviors, including all “classical” Pomeau-Manneville types I, II, and III intermittency, crisis-induced intermittency, and on-off intermittency, was found. We were able to identify each of these types, qualitatively from direct manifestation of the bifurcation properties in time series data, quantitatively from reconstructed return maps or from the scaling-laws occurring in the distribution and control-parameter dependence of the laminar lengths. As a result, it is demonstrated that the spin-wave experiment renders an excellent possibility to study intermittency in a real experimental situation. Moreover, we were able to attain important physical understanding from the analysis of intermittency, e.g., the occurrence of on-off intermittency in the coincidence regime gives a strong hint how new degrees of freedom could add to the system dynamics. Finally, new concepts in experimental nonlinear dynamics that are based on the intermittent switching between bistable or multistable states can be nicely studied in our system. A recent example refers to “noise-free” stochastic resonance [35] which was observed in conjunction with type-III intermittency under subsidiary absorption.

## ACKNOWLEDGMENTS

This project of SFB 185 ‘‘Nichtlineare Dynamik’’ Frankfurt/Darmstadt was partially financed by special funds of the Deutsche Forschungsgemeinschaft. We thank B. Bischof and E. Reibold for technical support and helpful comments.

## APPENDIX: DERIVATION OF INTERMITTENCY CHARACTERISTICS FROM THE EQUATION OF MOTION

A physical understanding of the observed intermittency phenomena requires that their specific mechanisms (e.g., the local or global bifurcations) can be related to the underlying parametric process described by Eq. (1). To give examples, we present analytical derivations of such bifurcations for the Pomeau-Manneville type-II intermittency, and for on-off intermittency. Note that in both cases our experimental data were taken under such conditions (see the discussion in Ref. [11]) that the excited modes participating in the nonlinear mechanism are of plain spin-wave type with relatively large wave numbers of the order of  $10^5 \text{ cm}^{-1}$ . This implies that the nonlinear coupling coefficients are essentially diagonal in  $\mathbf{k}$ :  $\rho_{\mathbf{k}\mathbf{k}'} \approx \rho_{\mathbf{k}\mathbf{k}} \delta_{\mathbf{k}\mathbf{k}'}$ , and Eq. (1) simplifies to

$$\dot{a}_0(t) = -[i\Delta\omega_0 + \Gamma_0]a_0 - \sum_{\mathbf{k}} \rho_{\mathbf{k}\mathbf{k}}^* a_{\mathbf{k}}^2 - i\gamma h, \quad (\text{A1})$$

$$\dot{a}_{\mathbf{k}}(t) = -[i\Delta\omega_{\mathbf{k}} + \Gamma_{\mathbf{k}}]a_{\mathbf{k}} + \rho_{\mathbf{k}\mathbf{k}} a_0 a_{\mathbf{k}}^*,$$

where the abbreviations  $\Delta\omega_0 \equiv \omega_0 - \omega_p$  and  $\Delta\omega_{\mathbf{k}} \equiv \omega_{\mathbf{k}} - \omega_p/2$  have been used. We just mention that the complex phase of the coupling coefficient can be absorbed in a redefinition of the magnon amplitudes  $a_{\mathbf{k}}$ , so that the  $\rho_{\mathbf{k}\mathbf{k}}$  may be considered as real quantities.

## 1. Pomeau-Manneville type II

In order to show that Eq. (A1) supports Pomeau-Manneville intermittency of type II, one has to prove the occurrence of a subcritical Hopf bifurcation. To this end we consider an even more simplified form of Eq. (A1) where the uniform mode interacts with only *one* spin-wave mode. For this simple two-mode model a nontrivial stable fixed point has been reported to occur at  $\gamma h = \sqrt{\Gamma_0^2 + \Delta\omega_0^2}/|\rho_{\mathbf{k}\mathbf{k}}|$  [36] in the specific case of resonant parametric pumping  $\Delta\omega_{\mathbf{k}} = 0$ . In the general nonresonant case, however, the stability of the nontrivial steady state  $a_0 = a_0^S, a_{\mathbf{k}} = a_{\mathbf{k}}^S \neq 0$  may be affected by stronger pumping. Looking for the linear stability of the nontrivial fixed point, one has to solve in general a characteristic equation of the fourth degree, since the two-mode model is in general characterized by four degrees of freedom, e.g., the amplitude and phase of either mode. To keep the problem analytically tractable, we applied a perturbation method with respect to the dimensionless parameters  $g \equiv \Gamma_0/\Gamma_{\mathbf{k}}$  and  $|c_{\mathbf{k}}|^2 \equiv |\rho_{\mathbf{k}\mathbf{k}} a_{\mathbf{k}}^S/\Gamma_{\mathbf{k}}|^2$ . At order zero the eigenvalues read  $\lambda_{1,2} = \pm i\Delta\omega_0, \lambda_3 = -2\Gamma_{\mathbf{k}}$ , and  $\lambda_4 = 0$ . In first order of perturbation we obtain

$$\lambda_{1,2} = \pm i\Delta\omega_0 - g\Gamma_{\mathbf{k}} + 2|c_{\mathbf{k}}|^2 \Gamma_{\mathbf{k}} \frac{\Gamma_{\mathbf{k}}^2}{\Delta\omega_0^2(4\Gamma_{\mathbf{k}}^2 + \Delta\omega_0^2)} \times \{ -\Delta\omega_0^2 + 2(-\Delta\omega_0\Delta\omega_{\mathbf{k}}) \pm i\Delta\omega_0[2\Gamma_{\mathbf{k}}^2 + \Delta\omega_0^2 - (-\Delta\omega_0\Delta\omega_{\mathbf{k}})]/\Gamma_{\mathbf{k}} \}, \quad (\text{A2})$$

$$\lambda_4 = -4\Gamma_{\mathbf{k}}|c_{\mathbf{k}}|^2(-\Delta\omega_0\Delta\omega_{\mathbf{k}})/(2\Delta\omega_0^2), \quad (\text{A3})$$

while  $\lambda_3$  remains negative. In order to have a Hopf bifurcation the real part of the complex conjugate pair  $\lambda_1 = \lambda_2^*$  has to change from negative to positive value, while  $\lambda_4 < 0$ . Both conditions require the inequality  $2(-\Delta\omega_0\Delta\omega_{\mathbf{k}}) \geq \Delta\omega_0^2 > 0$ , with the Hopf bifurcation occurring at  $|c_{\mathbf{k}}|^2/g = \Delta\omega_0^2(4\Gamma_{\mathbf{k}}^2 + \Delta\omega_0^2)/[4(-\Delta\omega_0\Delta\omega_{\mathbf{k}}) - 2\Delta\omega_0^2\Gamma_{\mathbf{k}}^2]$ . The latter condition implicitly yields a condition for the driving amplitude. The distinction between subcritical and supercritical bifurcation is related to the sign of the real part of the cubic coefficient in the (complex valued) Hopf normal form,  $\dot{z} = \lambda_1 z + R|z|^2 z$ . After some straightforward but lengthy algebra we obtain

$$\text{Re } R = \frac{8|c_{\mathbf{k}}|^2 \Gamma_{\mathbf{k}}^2 [2(-\Delta\omega_0\Delta\omega_{\mathbf{k}}) - \Delta\omega_0^2]}{(-\lambda_4)\Delta\omega_0^2 [4\Gamma_{\mathbf{k}}^2 + \Delta\omega_0^2]^2} \times [\Gamma_{\mathbf{k}}^2 + (-\Delta\omega_0\Delta\omega_{\mathbf{k}}) - \Delta\omega_{\mathbf{k}}^2]. \quad (\text{A4})$$

The sign of the real part is determined by the last factor. Thus the change from the supercritical to subcritical bifurcation occurs at

$$\Gamma_{\mathbf{k}}^2 + (-\Delta\omega_0\Delta\omega_{\mathbf{k}}) - \Delta\omega_{\mathbf{k}}^2 = 0. \quad (\text{A5})$$

Moreover one has to realize that the proper type of bifurcation is a condition necessary but not sufficient for the occurrence of intermittency, because of the related reinjection mechanism. This part of the problem can only be analyzed by numerical simulations in most cases. We refer to previous simulations on multimode models [37], which, in fact, yielded different kinds of intermittent behaviors including type-III and on-off intermittency.

## 2. On-off intermittency

The essential feature of on-off intermittency is the additional degree of freedom becoming unstable via a global symmetry-breaking bifurcation. Consider a set of spin waves interacting with each other through the uniform mode and forming a chaotic ensemble. In terms of a multimode model (A1), the coupling between the uniform mode  $a_0$  (the ‘‘chaotic mode’’) and any other spin wave  $a_{\mathbf{q}}$  not being initially in the ensemble is governed by

$$\dot{a}_{\mathbf{q}}(t) = -[i\Delta\omega_{\mathbf{q}} + \Gamma_{\mathbf{q}}]a_{\mathbf{q}} + \rho_{\mathbf{q}\mathbf{q}} a_0 a_{\mathbf{q}}^*. \quad (\text{A6})$$

By virtue of the chaotic dynamics of  $a_0$ , the mode  $a_{\mathbf{q}}$  may be parametrically excited, giving rise to intermittent oscillations. As usual in parametric instabilities an analytical expression for the corresponding threshold is difficult to obtain. If one models the chaotic dynamics of  $a_0$  by a Gaussian white noise,  $\langle a_0(t)a_0^*(t) \rangle = |a_0|^2 \delta(t)$ , then the threshold for in-

termittency is obtained as  $|\overline{a_0}|^2 = \Gamma_{\mathbf{q}} / |\rho_{\mathbf{q}\mathbf{q}}|^2$ . Contrary to simple models of on-off intermittency, the mechanism for the saturation of the spin wave amplitude is here not related to nonlinear contributions but may come from a dephasing mechanism developed in the context of the  $S$  theory.

Altogether, it is possible that a certain spin wave  $a_{\mathbf{q}}$  which has a vanishing amplitude below some critical value of the

control parameter, becomes visible in the global system dynamics above a threshold. The numerical results of Ref. [32] indicate that on-off intermittency seems to be a quite common phenomenon in such systems. The only additional condition is the absence of other attractors outside the invariant manifold. In this case the diffusionlike dynamics might ensure reinjection, and the intermittent behavior can occur.

- 
- [1] T.L. Carroll, L.M. Pecora, and F.J. Rachford, *Phys. Rev. A* **40**, 377 (1989), and references therein.
- [2] H. Benner, F. Rödelsperger, and G. Wiese, in *Nonlinear Dynamics in Solids*, edited by H. Thomas (Springer, Berlin, 1992), p. 129.
- [3] *Nonlinear Phenomena and Chaos in Magnetic Materials*, edited by P.E. Wigen (World Scientific, Singapore, 1994).
- [4] F.M. de Aguiar, *Phys. Rev. A* **40**, 7244 (1989).
- [5] F. Rödelsperger, Th. Weyrauch, and H. Benner, *J. Magn. Magn. Mater.* **104**, 1075 (1992).
- [6] F. Rödelsperger, *Chaos und Spinwelleninstabilitäten* (Verlag Harri Deutsch, Frankfurt, 1994).
- [7] H. Suhl, *J. Phys. Chem. Solids* **1**, 209 (1957).
- [8] G. Wiese and H. Benner, *Z. Phys. B* **79**, 119 (1990).
- [9] C.E. Patton and W. Jantz, *J. Appl. Phys.* **50**, 7082 (1979).
- [10] G. Wiese, H.-A. Krug von Nidda, and H. Benner, *Europhys. Lett.* **15**, 585 (1991).
- [11] H.-A. Krug von Nidda, G. Wiese, and H. Benner, *Z. Phys. B* **95**, 55 (1994).
- [12] H.G. Schuster, *Deterministic Chaos: An Introduction*, 2nd ed. (Physik-Verlag, Weinheim, 1988).
- [13] S. Newhouse, D. Ruelle, and F. Takens, *Commun. Math. Phys.* **64**, 35 (1978).
- [14] G. Gibson and C. Jeffries, *Phys. Rev. A* **29**, 811 (1984).
- [15] F.M. de Aguiar and S.M. Rezende, *Phys. Rev. Lett.* **56**, 1070 (1986).
- [16] Y. Pomeau and P. Manneville, *Commun. Math. Phys.* **74**, 189 (1980).
- [17] Type-I and -III intermittencies have, e.g., been found in simulations of a two-mode model with four-magnon couplings as well as in a model of two coupled classical spins; see F.M. de Aguiar, S.M. Rezende, F.C.S. da Silva, and A. Azevedo, *J. Magn. Magn. Mater.* **140-144**, 1933 (1995); S.M. Rezende and F.M. de Aguiar, *Phys. Lett. A* **208**, 286 (1995).
- [18] J.E. Hirsch, B.A. Huberman, and D.J. Scalapino, *Phys. Rev. A* **25**, 519 (1982).
- [19] C. Grebogi, E. Ott, and J.A. Yorke, *Phys. Rev. Lett.* **48**, 1507 (1982).
- [20] C. Grebogi, E. Ott, and J.A. Yorke, *Physica D* **7**, 181 (1983).
- [21] C. Grebogi, E. Ott, F. Romeiras, and J.A. Yorke, *Phys. Rev. A* **36**, 5365 (1987).
- [22] A.S. Pikovsky, *Z. Phys. B* **55**, 149 (1984).
- [23] H. Fujisaka and H. Yamada, *Prog. Theor. Phys.* **74**, 918 (1985); **75**, 1087 (1986).
- [24] N. Platt, E.A. Spiegel, and C. Tresser, *Phys. Rev. Lett.* **70**, 279 (1993).
- [25] E. Ott and J. C. Sommerer, *Phys. Lett. A* **188**, 39 (1994).
- [26] A.S. Pikovsky and P. Grassberger, *J. Phys. A* **24**, 4587 (1991);
- [27] A. Čenys, A. Anagnostopoulos, and G. Bleris, *Phys. Lett. A* **224**, 346 (1997).
- [28] J.F. Heagy, N. Platt, and S.M. Hammel, *Phys. Rev. E* **49**, 1140 (1994).
- [29] F. Rödelsperger, A. Čenys, and H. Benner, *Phys. Rev. Lett.* **75**, 2594 (1995).
- [30] A. Čenys and H. Lustfeld, *J. Phys. A* **29**, 11 (1996).
- [31] A. Čenys, A. Anagnostopoulos, and G. Bleris, *Phys. Rev. E* **56**, 2592 (1997).
- [32] A. Krawiecki and A. Sukiennicki, *Acta Phys. Pol.* **88**, 269 (1995).
- [33] F.T. Arecchi, R. Badii, and A. Politi, *Phys. Rev. A* **29**, 1006 (1984).
- [34] Th. Greiner, E. Reibold, and H. Benner (unpublished).
- [35] E. Reibold, W. Just, J. Becker, and H. Benner, *Phys. Rev. Lett.* **78**, 3101 (1997).
- [36] T. Walter, F. Rödelsperger, and H. Benner, *Z. Angew. Math. Phys.* **47**, 515 (1996).
- [37] F. Rödelsperger, Diploma thesis, TH Darmstadt, 1989.